A theory of Tesla disc turbines

Sayantan Sengupta and Abhijit Guha

Abstract

In the present article, a mathematical theory for the flow field within a Tesla disc turbine has been formulated in the appropriate cylindrical co-ordinate system. The basis of the theory is the Navier–Stokes equations simplified by a systematic order of magnitude analysis. The presented theory can compute three-dimensional variation of the radial velocity, tangential velocity and pressure of the fluid in the flow passages within the rotating discs. Differential equations as well as closed-form analytical relations are derived. The present mathematical theory can predict torque, power output and efficiency over a wide range of rotational speed of the rotor, in good agreement with recently published experimental data. The performance of the turbine is characterized by conceptualizing the variation of load through the non-dimensional ratio of the absolute tangential velocity of the jet and the peripheral speed of the rotor. The mathematical model developed here is a simple but effective method of predicting the performance of a Tesla disc turbine along with the three-dimensional flowfield within its range of applicability. A hypothesis is also presented that it may be possible to exploit the effects of intelligently designed and manufactured surface roughness elements to enhance the performance of a Tesla disc turbine.

Introduction

Tesla turbine, a bladeless turbine, was patented by the famous scientist Nikola Tesla (1856–1943) in 1913.[1] Up to now, a major stumbling block in its commercial use has been its low efficiency and certain other operational difficulties.[2] However, there has been a resurgence of research interest in this type of turbines[3] because they have several advantages (as explained below) and hence may be appropriately developed and used in certain niche application areas. In this article, an analytical theory has been developed for predicting the performance of Tesla turbines, which agree well with experimental results.

The Tesla turbine is also known as disc turbine because the rotor of this turbine is formed by a series of flat, parallel, co-rotating discs, which are closely spaced and attached to a central shaft.[2] The working fluid is injected nearly tangentially to the rotor by means of inlet nozzle. The injected fluid, which passes through the narrow gaps between the discs, approaches spirally towards the exhaust port located at the centre of each disc. The viscous drag force, produced due to the relative velocity between the rotor and the working fluid, causes the rotor to rotate. There is a housing surrounding the rotor, with a small radial and axial clearance.

Tesla turbine has several important advantages: it is easy to manufacture, maintain and balance the turbine, and it has high power to weight ratio, low cost, significant reduction in emissions and noise level, a simple configuration which means an inexpensive motor. Tesla turbine can generate power for a variety of working media[3] like Newtonian fluids, non-Newtonian fluids, mixed fluids, particle laden two-phase flows (many aspects of two-phase flow may be found in Guha[4,5]). This turbine has self-cleaning nature due the centrifugal force field. This makes it possible to operate the turbine in case of non-conventional fuels like biomass which produce solid particles. It also suggests that this bladeless turbine can be well suited to

---

Mechanical Engineering Department, Indian Institute of Technology Kharagpur, India

Corresponding author:
Abhijit Guha, Mechanical Engineering Department, Indian Institute of Technology Kharagpur, Kharagpur 721302, India.
Email: a.guha@mech.iitkgp.ernet.in

generate power in geothermal power stations.[6] Tesla turbo-machinery can also be used as a compressor by modifying the housing and powering the rotor from an external source. Moreover, it can operate either in the clockwise or anticlockwise direction.

However, a Tesla disc turbine has not yet been used commercially due to its low efficiency and other operational difficulties.[2] Further research and modification of Tesla turbine were temporarily suppressed after the invention of gas turbine which was much more efficient than Tesla turbine. From 1950 onwards both theoretical and experimental research on Tesla turbine, Tesla pump, Tesla fan and Tesla compressor has been regenerated.[7] Quite a number of analytical models for the conventional configuration of Tesla turbine have been developed. Among all these approaches available in the literature, bulk parameter analysis,[8–10] truncated series substitution methodology,[11] integral method,[12] and finite difference solutions[13,14] are worth mentioning. Solutions are mainly available for incompressible flows although there are some papers containing solutions for compressible flows.[15,16]

Currently the field of micro-turbine is an active research area; the bladeless Tesla turbine because of its simplicity and robustness of structure, low cost and comparatively better operation at high rpm may become a suitable candidate for this application. For this to happen the efficiency of the Tesla turbine, however, has to be improved. Researchers are attempting to achieve this by modification of the configuration of the conventional Tesla turbines (see, for example, Guha and Smiley[3]).

After the success of Whittle and von Ohain, the gas turbine became the centerpoint of research and development and the understanding of its performance and optimization has reached quite a mature stage.[17–23] The understanding of the performance of Tesla turbines is not nearly as thorough. The present authors would argue that the development of a reliable and comprehensive (and yet simple, if possible, for practical engineering use) mathematical theory is an important step towards developing the necessary understanding of the fluid dynamics of the Tesla disc turbine.

The objective of the present work is to formulate a mathematical theory for a Tesla turbine, developed in the appropriate cylindrical co-ordinate system. The geometric and flow configuration for the present study is chosen to be the same as that given in Lemma et al.[24] because they provide data from their recent experiments which can be used to verify the mathematical model and for the claimed superiority in its performance. Their experimental results show that this particular configuration of Tesla turbine has an isentropic efficiency of about 18–25% which is achieved by using rotor with only nine discs (diameter 0.05 m) and

compressed air as the working fluid. More details about the configuration are discussed later.

Deam et al.[25] have attempted to develop a simple analytical model for the configuration given in Lemma et al.,[24] considering incompressible and one dimensional flow. A limitation of their theory is the absence of the radial flow feature. Moreover, their theory can only predict the no-loss maximum efficiency of the turbine (assuming the fluid is flown through a duct with uniform cross section between a pressure reservoir and the atmosphere). In their theory[25] the no-loss maximum efficiency is attainable when the rotor velocity is equal to the velocity of the working fluid. This, however, does not happen in reality because, if there is no relative velocity between the disc-rotor and the working fluid, the viscous drag force will be zero and in consequence, there will be no power output. The scope of the present work is to develop an analytical model for a more realistic case considering three-dimensional flow and consequences of the viscous drag force. The model can compute the three-dimensional variation of the radial velocity, tangential velocity and pressure of the fluid in the flow passages within the rotating discs. Differential equations as well as closed-form analytical relations have been derived. The present mathematical model can predict torque, power output and efficiency over a wide range of rotational speed of the rotor.

Mathematical analysis

In this section, a new mathematical theory for the performance of Tesla turbine is formulated. The flow configuration used for this purpose is the same as that of Lemma et al.[24]

Description of the flow path

The domain for the mathematical solution is the three-dimensional space (Figure 1) between two circular rotor discs separated axially (i.e. in the z-direction) by a distance b. The rotor inlet is situated along the periphery of the discs (i.e. at radius r_2). The rotor outlet is at the centre of the discs (at radius r_1). Surrounding the rotor, there is a plenum chamber, the area of which reduces such that flow rate is uniform throughout the periphery. This signifies that at the rotor inlet both tangential and radial components of the velocity are uniform (i.e. the velocities are not a function of θ).

Viscous drag and its consequences

For establishing the mathematical model of the Tesla turbine the flow physics through the rotor discs should be well understood. The basic principle is that the viscous drag force between a solid and a fluid acts in the
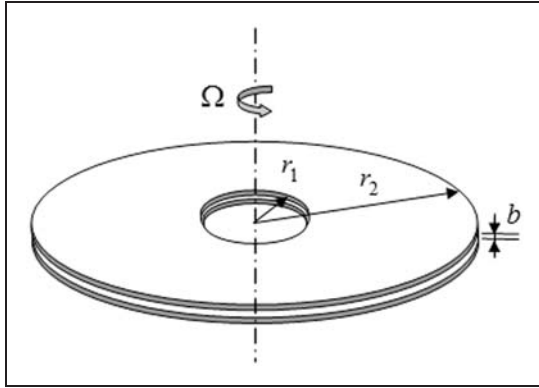
Figure 1. Schematic diagram of the domain for the mathematical solution. (The gap within the two discs, in relation to the radius, is exaggerated in the sketch for clarity).

direction of the relative velocity of the fluid. Suppose a solid object is moving at a velocity U through a stationary fluid. As the relative velocity of the fluid is $-U$, therefore the viscous drag force opposes the motion of the solid object. Now, consider a case when the fluid as well as the solid moves at the same velocity U. The relative velocity of the fluid is zero, hence there will be no viscous drag force. If the fluid and the solid move in the same direction, their absolute velocities being V and U respectively, then the condition $(V - U) > 0$ would mean that the relative velocity of the fluid is positive: the viscous drag force will therefore try to enhance the velocity of the solid in this case. This is what happens in the Tesla disc turbine. As the turbine starts from stationary condition, the fluid enters nearly tangentially at a high velocity into the stationary rotor through the outer periphery of the discs. So the drag force on the discs of the rotor will act in the direction of fluid flow. Since there is a relative velocity between the working fluid and the disc wall there exists a velocity gradient near the wall. This velocity gradient is responsible for the generation of shear stress which in turn develops a torque on the rotor. If this torque is greater than the frictional torque, the rotor will start rotating. As the rotor speed increases, the relative velocity of the fluid with respect to the disc decreases. This gradually decreases the angular acceleration of the rotor. Ultimately a steady state will arise when the rotor rotates at a constant speed at which the frictional torque is just balanced by the torque produced. If the turbine is loaded, the rotational speed of the rotor at steady state will be less than the steady rotational speed at no load for the same inlet condition. This implies that at steady state the relative tangential velocity of the working fluid with respect to the discs will increase when the load on the turbine increases. This concept has been utilized in this work to calculate the power output at different steady states, under various load conditions.

Assumptions

The working fluid leaving from nozzle has a high linear momentum. This linear momentum transforms into angular momentum in the plenum chamber. The fluid has mainly tangential and radial velocities while it enters through the narrow gap between the discs.

As the fluid moves towards the center of the discs, its radial velocity increases due to the gradual decrease of the flow area. The fluid follows a spiral path from the inlet up to the central exit. To visualize this process clearly, the fluid pathlines were computed numerically by Lagrangian tracking calculations performed by the commercially available computational fluid dynamics (CFD) software Fluent 6.3. Figure 2 shows the results of such computations, where spiral paths lines for 2.77×10^4 fluid particles are superposed.

In order to make the complex flow amenable to an analytical theory, a few assumptions are made: (1) the fluid is Newtonian with constant properties, (2) the flow is steady, (3) the flow is axisymmetric, (4) axial (z-direction) velocity is negligible compared to the radial and tangential velocities, (5) radial gradients are smaller than the axial gradients, (6) body forces along r and θ directions are negligible, (7) the flow is laminar, (8) flow characteristics between any two discs of the rotor are the same. Hence a theoretical model of the flow between two discs is developed here. The torque and power developed by the flow through two discs can then be calculated. The total torque and power from the whole rotor assembly are then calculated by the multiplying these quantities for one inter-disc gap with the number of inter-disc gaps available.

Since the gap between two consecutive discs is very small compared to other dimensions of the disc (Figure 1), the vena-contracta effect at entry has not been included in the analysis here. The fluid dynamics of the flow at the exit from the inter-disc gaps is complex – Hoya and Guha[2] have given an extensive discussion of this topic. Accurate determination of the loss due to this complex exit flow is difficult and work is in progress to develop a quantitative prediction method. It is also assumed here that the surface of the disc is smooth. However, there are a large number of recent experimental and numerical studies which show that roughness elements can strongly affect the flow through a micro-channel (the small gap between two adjacent discs may make the flow domain in a Tesla turbine a "micro-channel"). These references suggest that the surface roughness elements can reduce the flow transition Reynolds number, enhance frictional drag, i.e. wall shear stress (more so than their effect in
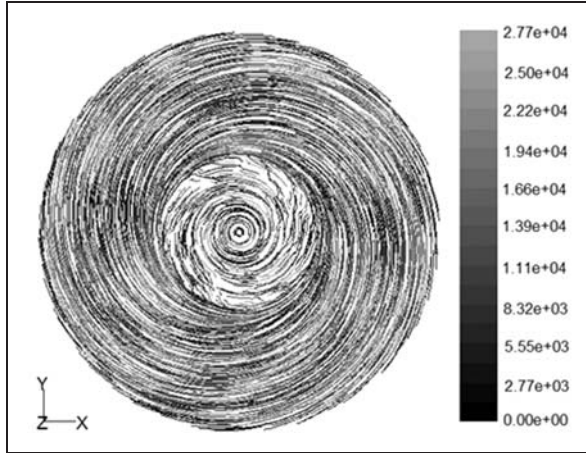
Figure 2. Fluid path lines computed in Fluent colored by particle ID in grey scale.

macro-channels), and alter the velocity profile. Kandilikar et al.,[26] for example, extended the conventional Moody diagram to values of relative roughness greater than 0.05 and showed that flow constriction effect in micro-channel becomes important when the relative roughness is greater than 0.05. Other than the relative roughness which gives a simple average measure of the height of the roughness elements, the spectrum of sizes, shapes and orientations of the roughness elements and their spatial distribution would affect the detailed fluid dynamics, including the velocity profile and wall shear stress, of the flow within the inter-disc gaps of a Tesla turbine. These flow features would be included in a more comprehensive theoretical treatment in the future. It follows from this discussion that it may be possible to exploit the effects of intelligently designed and manufactured surface roughness elements to enhance the performance of a Tesla disc turbine.

Mathematical formulation

The analysis begins with the Navier–Stokes equations in the cylindrical co-ordinate system. The continuity equation, the momentum equations and boundary conditions are written in terms of relative velocities. For this purpose the following relations between the absolute and relative velocities are used. $U_r = V_r$; $U_z = V_z$; $U_\theta = (V_\theta + \Omega * r)$. Using the assumptions listed above and an order of magnitude analysis (Appendix 2), the conservation equations take the following simplified form

$$\text{Continuity equation } \frac{\partial V_r}{\partial r} + \frac{V_r}{r} = 0 \tag{1}$$

$$\theta - \text{Momentum equation } V_r \frac{\partial V_\theta}{\partial r} + \frac{V_r V_\theta}{r} + 2\Omega V_r$$
$$= \nu \frac{\partial^2 V_\theta}{\partial z^2} \tag{2}$$

$$r - \text{Momentum equation } V_r \frac{\partial V_r}{\partial r} - \Omega^2 r - 2\Omega V_\theta - \frac{V_\theta^2}{r}$$
$$= -\frac{1}{\rho} \frac{dp}{dr} + \nu \frac{\partial^2 V_r}{\partial z^2} \tag{3}$$

$$z - \text{Momentum equation } \frac{\partial P}{\partial z} = 0 \tag{4}$$

Boundary conditions

$$\text{at } r = r_2 \quad \overline{V}_r = \overline{V}_{r_2} \quad \overline{V}_\theta = \overline{V}_{\theta_2} \tag{5}$$

$$\text{at } z = 0 \quad V_r = 0 \quad V_\theta = 0 \tag{6}$$

$$\text{at } z = b \quad V_r = 0 \quad V_\theta = 0 \tag{7}$$

$$\text{at } z = b/2 \quad \frac{\partial V_r}{\partial z} = \frac{\partial V_\theta}{\partial z} = 0 \tag{8}$$

Within the boundary layer developed on the flat solid discs, the relative tangential and radial velocities at any radius between r_1 and r_2 can be modelled as

$$V_\theta(r, z) = \overline{V}_{\theta_2} \zeta(R) G(z) \tag{9}$$

$$V_r(r, z) = \overline{V}_{r_2} \xi(R) H(z) \tag{10}$$

where,

$$R = \frac{r}{r_2}, \quad \zeta(R) = \frac{\overline{V}_\theta(r)}{\overline{V}_{\theta_2}}, \quad \xi(R) = \frac{\overline{V}_r(r)}{\overline{V}_{r_2}}$$
$$G(z) = \frac{V_\theta(r, z)}{\overline{V}_\theta(r)}, \quad H(z) = \frac{V_r(r, z)}{\overline{V}_r(r)}$$

G and H are respectively the z-variation of tangential and radial velocities within the boundary layers. Here we assume that the velocity profile of the fully developed flow is parabolic in nature. Accordingly, G and H are as expressed as

$$G = 6 * \frac{z}{b} \left(1 - \frac{z}{b}\right) \tag{11}$$

$$H = 6 * \frac{z}{b} \left(1 - \frac{z}{b}\right) \tag{12}$$

where b is the gap between the two discs. For a throughflow situation (i.e. when the inlet velocity is in the radial direction), Matveev and Pustovalov[27] and

Boyd and Rice[14] had assumed the same relation as equation (12) for the variation of the radial velocity.

The computed torque and power from the present theory will depend strongly on the variation of the tangential component of the velocity (hence on G through equation (11)). Therefore, in order to assess the validity of equation (11), a numerical simulation of the flow through two discs is carried out here with the help of the software Fluent 6.3. The flow geometry for this numerical simulation is taken to be the same as that of the experimental set up of Lemma et al.[24] For this numerical simulation, each disc has an outer radius of 25 mm and an inner radius of 13.2 mm, and a rotational speed of 1000 rad/s for the two discs is used. At inlet, the tangential velocity is specified as 106 m/s and the radial velocity is −11.5 m/s. Outlet boundary condition at central exit is modelled as pressure outlet with zero gauge pressure. No slip boundary condition is set on the disc walls. A grid-independence test has been carried out by grid adaptation technique. A total of 9,652,417 tetrahedral computational cells are used for the results presented below.

The tangential velocity computed by Fluent is shown in Figure 3 at three representative radial locations. The corresponding values of the tangential velocity as predicted by the assumed relation (equation (11)) are also shown in the same figure for a direct comparison. Since the torque (and hence the power) depends on the axial gradient of the relative tangential velocity ($\partial V_\theta / \partial z$), the corresponding quantity from the Fluent simulation ($\partial U_\theta / \partial z$) is shown in Figure 4. The plot is given in the close vicinity of the solid wall to examine the details of the flow features that determine the wall shear stress. It can be seen from Figure 4 that, at all three radial locations, the variation of $\partial U_\theta / \partial z$ is linear. From Figures 3 and 4, it can be concluded that a parabolic variation (equation (11)) is an adequate representation at the close vicinity of the wall, which determines the shear stress at the wall.

Integration of the continuity equation

Equations (9) and (10) show that in order to determine V_r and V_θ completely, one needs to find out $\xi(R)$ and $\zeta(R)$. Integrating the differential form of the continuity equation (1), one can get $\xi(R)$.

$$\int_0^h \int_{r_2}^r \frac{\partial (r V_r)}{\partial r} \delta r \delta z = 0 \tag{13}$$

Equation (13) leads to

$$\xi(R) = \frac{\overline{V_r}(r)}{\overline{V}_{r_2}} = \frac{r_2}{r} \tag{14}$$

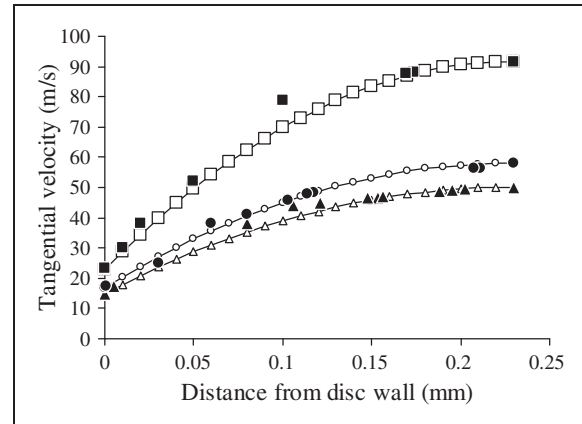**Figure 3.** Verification of one of the assumptions: comparison of assumed profile of tangential velocity with that predicted by Fluent.
Keys: —□— at a radius of 23 mm (equation 11), ■ at a radius of 23 mm (from Fluent), —○— at a radius of 17 mm (equation 11), ● at a radius of 17 mm (from Fluent), —△— at a radius of 15 mm (equation 11), ▲ at a radius of 15 mm (from Fluent).
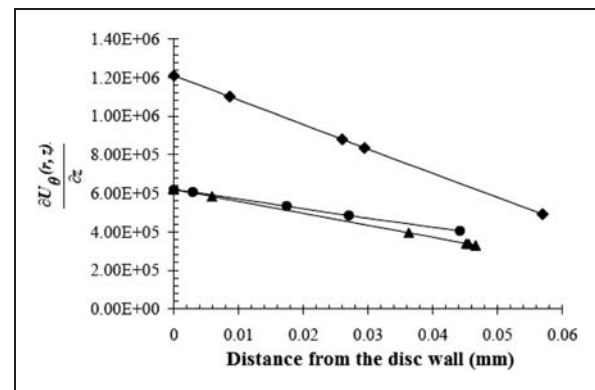

Figure 4. Verification of one of the assumptions: $\frac{\partial U_\theta(r,z)}{\partial z}$ versus distance from the disc wall, as computed by Fluent.
Keys: —◆— gradient calculated at a radius of 23 mm (close to inlet), —■— gradient calculated at a radius of 17 mm, —▲— gradient calculated at a radius of 15 mm (close to outlet).

Figure 5 shows the variation of ξ from inlet to the rotor up to the central exit. The value of ξ increases from the inlet to the central exit since the cross-sectional area varies inversely with radius. Figure 6 shows the three dimensional variation of non-dimensional radial velocity, as predicted by equation (10), in the domain of the mathematical solution.

Lemma et al.[24] produced a set of experimental results for which they had kept the nozzle inlet pressure fixed and varied the load so that the rotor attained the steady state at various values of the rotational speed Ω. The pressure drop through the rotor, Δp_{ic},
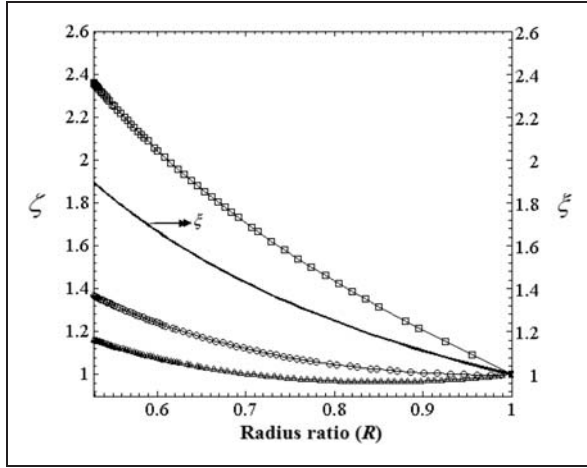
Figure 5. Prediction of the present theory for the variation of non-dimensional z-averaged relative velocity from inlet ($R = 1$) to central exit ($R = 0.528$) for various values of tangential speed ratio γ.
Keys for tangential component ζ: —□— $\gamma = 1.5$, —○— $\gamma = 3$, —△— $\gamma = 7$; Solid line represents radial component ξ for all γ. For all calculations $\Delta p_{ic} = 0.113$ bar.
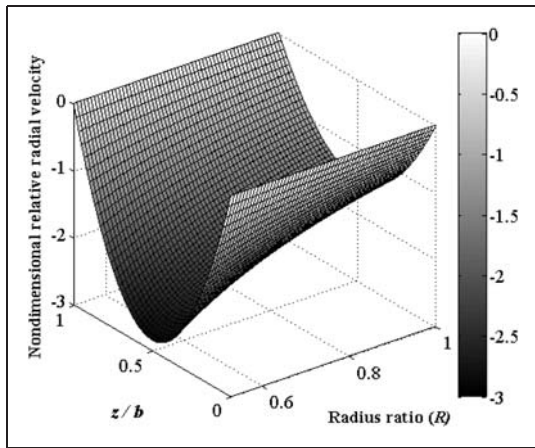

Figure 6. Prediction of the present theory for the variation of $\frac{V_r}{V_{r_2}}$ (non-dimensional relative radial velocity) in the three-dimensional domain. For all calculations, $\Delta p_{ic} = 0.113$ bar.

is a function of Ω as well as the mass flow rate through the rotor (i.e. $\overline{V}_{r_2}$). (See the prediction of the present theory later for a quantitative appreciation of this fact.) Δp_{ic} tends to increase with increasing Ω. Therefore, the mass flow rate (hence $\overline{V}_{r_2}$) would have to decrease correspondingly to keep Δp_{ic} fixed at a given value. Lemma et al.[24] measured this variation in $\overline{V}_{r_2}$ and found that, for a particular pressure drop between the rotor inlet and the central exit, $\overline{V}_{r_2}$ is maximum when the rotor is stationary and its magnitude

decreases linearly (up to 0.7 bar pressure drop) with Ω as given by:

$$-\overline{V}_{r_2} = A - B\Omega. \tag{15}$$

In equation (15), A is the maximum inlet radial velocity for stationary rotor, and B is the slope to be determined by the ratio of the maximum inlet radial velocity for stationary rotor (A) to the rotational speed of rotor for which no flow condition is arrived (Ω_0).

Integration of the r and θ momentum equations

We introduce the following three non-dimensional variables for further theoretical development

$$p' = \frac{p - p_2}{\rho\Omega^2 r_2^2}, \quad \phi_2 = \frac{\overline{V}_{r_2}}{\Omega r_2}, \quad \gamma = \frac{\overline{U}_{\theta_2}}{\Omega r_2} \tag{16}$$

The θ-momentum equation (2) is integrated partially (Appendix 3) with respect to z over the domain $(0, b/2)$, giving

$$\frac{d\zeta}{dR} = -\left\{\frac{1}{R} + 10 * \left(\frac{\nu}{\Omega b^2}\right) * \frac{R}{\phi_2}\right\}\zeta - \frac{10}{6(\gamma - 1)} \tag{17}$$

The r-momentum equation (3) is integrated partially (Appendix 3) with respect to z over the domain $(0, b/2)$, resulting in

$$\frac{dp'}{dR} = R + 2(\gamma - 1)\zeta + \frac{6}{5}(\gamma - 1)^2\frac{\zeta^2}{R} + \frac{6}{5}\frac{\phi_2^2}{R^3} - 12\left(\frac{\nu}{\Omega b^2}\right)\frac{\phi_2}{R} \tag{18}$$

Equation (15) is substituted in the equations (17) and (18) and these two ODEs are solved for the initial conditions given below

At $R = 1; \zeta = 1$ \hfill (19)

At $R = 1; p' = 0$ \hfill (20)

The solutions of the above two equations (17) and (18) will give ζ and p'. Equations (17) and (18) can be integrated simultaneously by numerical means. A simple iterative scheme may be adopted as follows. Assume a value of γ for which the steady state solution is sought. Start with a trial value of Ω. Equations (17) and (18) are then numerically integrated from the rotor inlet to the central exit. The computed value of the pressure drop will not, in general, agree with the

imposed value of Δp_{ic}. The value of Ω is then systematically varied until the iteration converges to the given value of Δp_{ic}. The same procedure is repeated for various values of γ.

It is noted that when γ is prescribed, equations (17) and (18) can be integrated analytically to find the variation of V_θ as well as Δp_{ic}. Analytical integration of equation (17) gives

$$\zeta = \frac{C_3}{R} + \frac{C_4 \exp\left[-\frac{C_1 R^2}{2}\right]}{R} \tag{21}$$

where

$$C_1 = \frac{10\nu}{\phi_2 \Omega b^2}, C_2 = \frac{-10}{6(\gamma-1)}, C_3 = \frac{C_2}{C_1}, C_4 = (1-C_3)\exp\left[\frac{C_1}{2}\right]$$

The variation in ζ from the rotor inlet to the central exit, for various values of γ, is shown in Figure 5. It can be observed from this figure that for lower values of γ (such as 1.5) ζ increases monotonically from inlet to the central exit; but for higher values of γ (such as 3, 7), ζ at first decreases then increases. This happens because there are two opposing effects that tend to change the value of ζ: ζ tends to decrease due to the effect of viscous drag (friction) and tends to increase due to the conservation of angular momentum. As it is discussed in the 'Viscous drag and its consequences' section viscous drag force is proportional to the relative tangential velocity of the working fluid (V_θ). For a high value of γ, the relative tangential velocity is high, therefore the effect of friction may supersede the effect of conservation of angular momentum. This is why, when γ is high, ζ initially decreases from the inlet up to a certain value of R at which ζ attains its minimum value. At lower values of R, ζ increases again as the effect of the angular momentum conservation starts to dominate. The three-dimensional variation of the non-dimensional relative tangential velocity V_θ is shown in Figures 7 and 8 for $\gamma = 1.5$ and $\gamma = 7$ respectively.

Substituting the expression of ζ from the equation (21) into the equation (18), $\frac{dp'}{dR}$ is calculated from the rotor inlet to the central exit for various values of γ. Figure 9 shows that the variation in $\frac{dp'}{dR}$ from $R=1$ (rotor inlet) to $R=0.528$ (central exit) at lower value of γ is less than that at higher value of γ.

Analytical integration of equation (18) gives

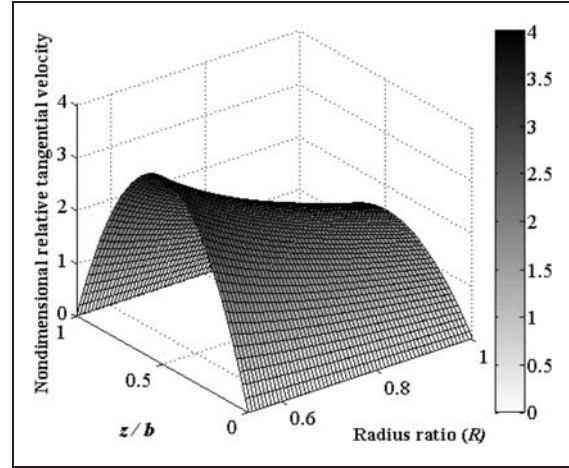$$p' = p'_k(R) + C_6 I_1 + C_8 I_2 + C_9 I_3 + C_{12} \tag{22}$$

Figure 7. Prediction of the present theory for the variation of $\frac{V_\theta}{V_{\theta_2}}$ (non-dimensional relative tangential velocity) in the three-dimensional domain. $\Delta p_{ic} = 0.113$ bar and $\gamma = 1.5$.

where

$$p'_k(R) = \frac{R^2}{2} + (C_5 + C_{11})\ln R - \frac{1}{2R^2}(C_7 + C_{10})$$

$$I_1 = \frac{1}{2}\left[\ln\left(\frac{-C_1 R^2}{2}\right) + \sum_1^\infty \frac{\left(\frac{-C_1 R^2}{2}\right)^{n+1}}{(n+1)(n+1)!}\right]$$

$$I_2 = \frac{C_1 \exp(-C_1 R^2)}{-2C_1 R^2} - \frac{C_1}{2}\left[\ln(-C_1 R^2) + \sum_1^\infty \frac{(-C_1 R^2)^{n+1}}{(n+1)(n+1)!}\right]$$

$$I_3 = \frac{C_1 \exp\left[-\frac{C_1 R^2}{2}\right]}{-2C_1 R^2} - \frac{C_1}{4}\left[\ln\left(\frac{-C_1 R^2}{2}\right) + \sum_1^\infty \frac{\left(\frac{-C_1 R^2}{2}\right)^{n+1}}{(n+1)(n+1)!}\right]$$

$$C_5 = 2(\gamma-1)C_3, C_6 = 2(\gamma-1)C_4$$

$$C_7 = \frac{6}{5}(\gamma-1)^2 C_3^2, C_8 = \frac{6}{5}(\gamma-1)^2 C_4^2$$

$$C_9 = \frac{12}{5}(\gamma-1)^2 C_3 C_4, C_{10} = \frac{6}{5}\phi_2^2, C_{11} = \frac{-12\nu\phi_2}{\Omega b^2}$$

$$C_{12} = -\left(p'_k(R) + C_6 I_1 + C_8 I_2 + C_9 I_3\right)_{R=R_1}$$

It is instructive to note here that at the central exit, $p = p_2$, therefore $p' = 0$; at inlet, $p' = \Delta p_{ic}/(\rho\Omega^2 r_2^2)$. It is to be remembered that Δp_{ic} was kept fixed for a given set of experiments;[24] this is how the numerical predictions of the present theory have been presented in various figures in order to be compatible with the experiments.
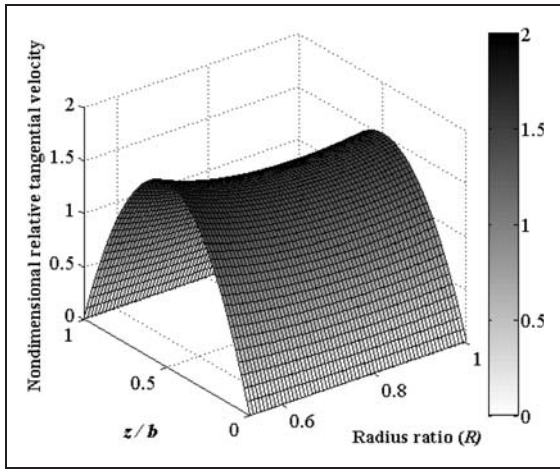
Figure 8. Prediction of the present theory for the variation of $\frac{V_\theta}{\overline{V}_{\theta_2}}$ (non-dimensional relative tangential velocity) in the three-dimensional domain. $\Delta p_{ic} = 0.113$ bar and $\gamma = 7$.
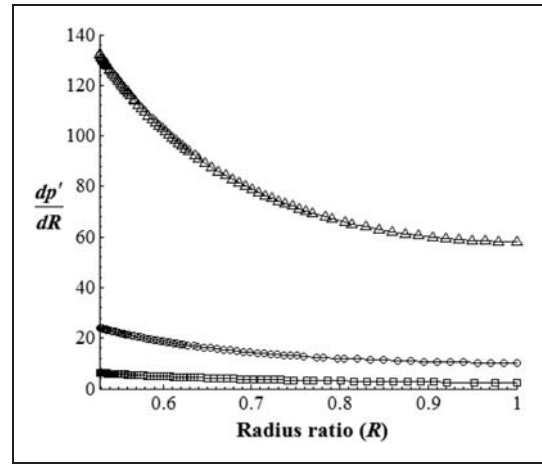

Figure 9. Prediction of the present theory for the variation of $\frac{dp'}{dR}$ from inlet ($R=1$) to central exit ($R=0.528$) for various values of tangential speed ratio γ. For all calculations $\Delta p_{ic} = 0.113$ bar Keys: —□— $\gamma = 1.5$, —◇— $\gamma = 3$, —△— $\gamma = 7$.

Calculation of power output and efficiency

$\zeta(R)$ is known from equation (21), hence $V_\theta(r, z)$ can be found out from equation (9). (This is how the variation in $V_\theta(r, z)$ has been plotted in Figures 7 and 8.) From the known distribution in tangential velocity, the total torque and power output of the rotor can be calculated by the following steps.

Wall shear stress on one side of a single disc is given by

$$\tau_w(r) = \left[\mu \frac{\partial V_\theta(r, z)}{\partial z}\right]_{at\ z=0} = \left[\mu \frac{\partial\{\overline{V}_{\theta_2}\zeta(R)G(z)\}}{\partial z}\right]_{at\ z=0}$$
$$= \frac{6\mu\overline{V}_{\theta_2}\zeta(R)}{b} \tag{23}$$

Consider an elemental circular strip of thickness dr at a radius r. The torque about the rotor axis of the shear force acting on this elemental area is equal to $\tau_w(2\pi r dr)(r)$. The torque on one side of a single disc can be calculated by integrating the elemental torque, and is given by

$$\Im = \int_{r_1}^{r_2} \tau_w(2\pi r)dr = \int_{r_1}^{r_2} \frac{6\mu\overline{V}_{\theta_2}\zeta(R)}{b}(2\pi r)dr$$
$$= \left(\frac{12\pi\mu\overline{V}_{\theta_2}r_2^3}{b}\right)\int_{R_1}^{R_2} R^2\zeta(R)dR$$
$$= \left(\frac{12\pi\mu\overline{V}_{\theta_2}r_2^3}{b}\right)\left[C_3(R_2^2 - R_1^2) - \frac{C_4}{C_1}\right.$$
$$\left.\times \left\{\exp\left(-\frac{C_1R_2^2}{2}\right) - \exp\left(-\frac{C_1R_1^2}{2}\right)\right\}\right] \tag{24}$$

The total torque produced by the complete rotor consisting of n_d discs is then calculated by

$$\Im_{tot} = 2(n_d - 1)\Im \tag{25}$$

The theoretical ideal power output is then given by

$$\dot{W}_{th} = \Im_{tot} * \Omega \tag{26}$$

As already explained after equation (20), Ω at any steady state is determined for a particular value of γ and a constant pressure drop Δp_{ic}. In the present theory, the variation of the load is conceptualized through γ – the non-dimensional ratio of the absolute tangential velocity of the jet and the peripheral speed of the rotor. If the load varies, γ at steady state will also vary. Therefore the power output changes with the change of load.

Theoretical power output with loss can be calculated by subtracting the loss from $\dot{W}_{th}$ given by equation (26)

$$\dot{W}_{act} = \dot{W}_{th} - \dot{W}_{loss} \tag{27}$$

where $\dot{W}_{loss}$ is the overall loss in power output. A Tesla disc turbine suffers from various kinds of losses; for example bearing loss, leakage loss, windage loss, losses due to irreversibility of nozzles, losses due to uncontrolled diffusion in the exhaust process, losses due to partial admission.[28] Leakage loss occurs due to the leakage flow through the bearing, seals and the clearance gaps between the rotor and the housing. Windage loss is due to the first and last disc rotating within a nearly stagnant fluid. Loss due to partial admission is caused because of finite thickness of the

discs and the interference of the edges of the discs. It is difficult to theoretically estimate the magnitude of each of these components of losses separately. In this work, therefore, an experimentally determined correlation for the overall loss is used.

Since the present theory is verified by comparing its predictions with the experimental measurements of Lemma et al.,[24] the experimental correlation for the overall loss provided in Lemma et al.,[24] i.e. $\dot{W}_{loss} \propto \Omega$, is used in the example calculations of isentropic efficiency (given later in 'Results and discussion' section). However, it should be noted that the experimental data of Lemma et al.[24] show a large degree of scatter and hence the accuracy of the linear correlation suggested by them is questionable.

A simple but very effective method for measuring the overall loss (the bearing and other losses), called the "angular acceleration method", has been developed in Hoya and Guha.[2] Their measurements showed that the frictional torque (for the turbine tested) was a non-linear function of Ω, the corresponding loss in power was therefore also a non-linear function of Ω (if the non-linearity in torque is expressed as a polynomial, the loss in power will then be a polynomial of higher order).

Efficiency of Tesla turbine. Hoya and Guha[2] have shown that, unlike the universal definition for efficiency of the turbine in a gas turbine plant, various researchers use different expressions for calculating the efficiency of Tesla turbines. One therefore needs to be careful in interpreting quoted values of efficiency of a Tesla turbine. Since the prediction of the present theory will be compared with the experiments of Lemma et al.,[24] their definition of the efficiency is adopted here

$$\eta = \frac{\dot{W}_{act}}{\dot{W}_{isentropic}} \tag{28}$$

The same expression for $\dot{W}_{isentropic}$ as used in Lemma et al.[24] is applied in equation (28) in the numerical example calculations given later. It is shown below that the definition used in Lemma et al.[24] for isentropic work is identical with what is used for a conventional turbomachinery if the change in kinetic energy is neglected. Noting that the inlet is denoted by suffix 2 and the outlet is denoted by suffix 1, one can then write

$$\dot{W}_{isentropic} = \dot{m}(h_2 - h_1) = \dot{m}c_p(T_2 - T_1)$$
$$= c_p \dot{m} T_1 \left(\frac{T_2}{T_1} - 1 \right) = \frac{k}{k-1} p_1 Q_1 \left[\left(\frac{p_2}{p_1} \right)^{\frac{k-1}{k}} - 1 \right] \tag{29}$$

where, Q is the total volume flow rate through all the inter-disc spaces and can be calculated from

$$Q = 2\pi r b (n_d - 1) \overline{V}_r \tag{30}$$

Condition for no torque. The net (integrated) effect of the jet on the disc becomes zero when $\int_{R_1}^{R_2} R^2 \zeta(R) dR = 0$; at this condition the jet produces no torque, and hence no power. By substituting the expression for ζ given by equation (21) into this condition and performing the integration one can show that the no torque condition arises at a particular value of γ given by

$$[\gamma]_{\text{no torque}}$$

$$= 1 - \frac{10}{6} \left[\frac{C_1(R_2^2 - R_1^2) + \exp\left(\frac{C_1}{2}\right)\left\{\exp\left(-\frac{C_1 R_2^2}{2}\right) - \exp\left(-\frac{C_1 R_1^2}{2}\right)\right\}}{C_1 \exp\left(\frac{C_1}{2}\right)\left\{\exp\left(-\frac{C_1 R_2^2}{2}\right) - \exp\left(-\frac{C_1 R_1^2}{2}\right)\right\}} \right] \tag{31}$$

Results and discussion

General predictions of the present theory have already been discussed in the sections 'Integration of the continuity equation' and 'Integration of the r and θ momentum equations'. The two-dimensional and three-dimensional variation of the three important parameters – V_r, V_θ and p' (relating to Δp_{ic}) – are shown in Figures 5 to 9.

In order to compare the present theory with experimental measurements, the following geometric and flow data are taken from Lemma et al.[24]: $r_1 = 13.2$ mm, $r_2 = 25$ mm, $n_d = 9$. For $\Delta p_{ic} = 0.113$ bar, overall loss in Watt = 0.0001635 * rpm, and the value of constants A, B in equation (15) required to calculate $\overline{V}_{r_2}$ are 13.32 and 0.0014, respectively.

For a particular pressure drop Δp_{ic} between the inlet and the central exit, if the load increases then the steady state rotational speed of rotor decreases from its highest value at no load condition. It has been explained in the 'Integration of the r and θ momentum equations' section how the steady state Ω is determined iteratively for given values of Δp_{ic} and γ. It has been described in the section 'Calculation of power output and efficiency', how the theoretical power output curve versus rotational speed can be constructed. Such prediction of theoretical power output is shown in Figure 10 for $\Delta p_{ic} = 0.113$ bar, where both the theoretical power outputs with and without loss are included. Each computed point in Figure 10 represents a steady state solution. In the same figure the experimental results of Lemma et al.[24] are also shown so that a direct comparison is possible. Considering the facts that there is
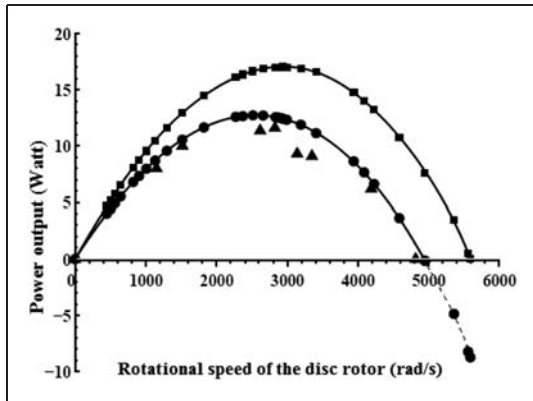
Figure 10. Comparison of the present theory with experiment: variation of the power output of Tesla turbine with rotational speed.
Keys: —■— Theoretical ideal power output, —●— Theoretical power output with loss, ▲ Experimental power output.[24] Each bullet represents a steady state. For all calculations and experiments $\Delta p_{ic} = 0.113$ bar.
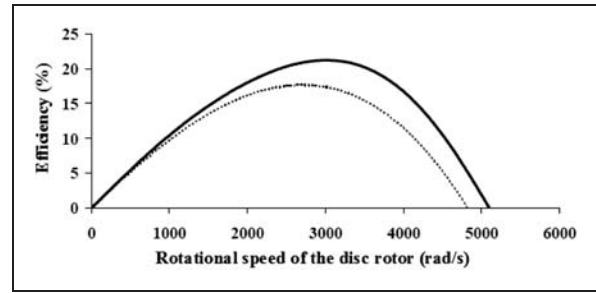

Figure 11. Comparison of the present theory with experiment: variation of the efficiency (%) of Tesla turbine with rotational speed.
Keys: —— Theoretical efficiency with loss as predicted by the present theory, · · · · Efficiency of Tesla turbine from the experiment.[24] For all calculations and experiments $\Delta p_{ic} = 0.113$ bar.

considerable experimental uncertainty and that the magnitude of the bearing and other losses is a very substantial fraction of the power output (Figure 10), it can be said that the simple theory developed here has worked well.

From simple theoretical considerations, Hoya and Guha[2] have shown that $\Im \approx \Im_0 - c\Omega$, where $\Im_0$ and c are constants, and therefore the theoretical power output is $\dot{W}_{th} = \Im\Omega = \Im_0\Omega - c\Omega^2$. This explains why the power versus rotational speed curves in Figure 10 show the general shape of inverted buckets and the power output produces a maxima. It can be seen that the rotational speed at which the maxima occurs is different for the two theoretical power output curves – the one which includes the loss and the other which does not. Equation (27), using the linear correlation for overall loss suggested by Lemma et al.,[24] therefore shows that $\dot{W}_{act} = \Im_0\Omega - c\Omega^2 - d\dot{\Omega}$, where d is another constant. Hence the maxima for $\dot{W}_{act}$ occurs at a lower rotational speed as compared to the maxima for $\dot{W}_{th}$. In this connection one should consider the discussion, regarding the validity of the linear correlation for overall loss, given in the 'Mathematical analysis' section. In particular, it may be noted that a simple but very effective method for measuring the overall loss (the bearing and other losses), called the "angular acceleration method", has been developed in Hoya and Guha.[2] Their measurements showed that the frictional torque (for the turbine tested) was a non-linear function of Ω, the corresponding loss in power was therefore also a non-linear function of Ω (if the non-linearity in torque is expressed as a polynomial, the loss in power will then be a polynomial of higher order).

Figure 10 shows that (for $\Delta p_{ic} = 0.113$ bar), the theoretical power output $\dot{W}_{th}$ is zero at 5592 rad/s. This occurs when $\gamma = 0.631$, (this corresponds to the condition when there is no torque because of the action of the fluid jet on the disc). $\Omega_{\text{no torque}} = 5592$ rad/s thus corresponds to the steady-state condition under no load. When the bearing and other parasitic losses are absent, the no torque condition, the no load condition and the no power condition all occur at the same steady rotational speed of the rotor. However, when bearing and other parasitic losses are present, an external agency will actually have to supply the power (that is equal to the losses) for the disc to rotate at the steady rotational speed of 5592 rad/s. This is shown as the negative power output in Figure 10. The power output with losses becomes zero at 4950 rad/s, but at this point the torque produced by the jet is non-zero.

Figure 11 shows the variation of the theoretical efficiency of the Tesla disc turbine over a range of rotational speed of the disc rotor. Like Figure 10, each computed point in Figure 11 represents a steady state solution. The maximum theoretical efficiency of the nine discs rotor at $\Delta p_{ic} = 0.113$ bar is 21%. A study of Figures 10 and 11 together shows that the point of maximum efficiency occurs at a slightly different rotational speed as compared to the point of maximum power: this is so because the denominator used in the particular definition of efficiency (equation (28)) also depends on the rotational speed (as revealed by a consideration of equations (29), (30) and (15)). In the same Figure 11, the experimental values from Lemma et al.[24] are superposed so that a direct comparison of the prediction of the present theory with experiments is possible. In the context described in the third paragraph of the 'Results and discussion' section, the present theory compares well with experiments.

Conclusion

A mathematical theory for the performance of a Tesla disc turbine has been formulated here. The basis of the theory is the Navier–Stokes equations simplified by a systematic order of magnitude analysis resulting in the present fundamental set of coupled differential equations (1) to (3) that govern the flow-field within a Tesla disc turbine. The theoretical model can compute the three-dimensional variation of the radial velocity, tangential velocity and pressure of the fluid in the flow passages within the rotating discs. The partial differential equations can be converted to ODEs by suitable assumptions regarding non-dimensional velocity profiles; the coupled set of ODEs (equations (17) and (18)) can be integrated by simple numerical schemes (section 'Integration of the r and θ momentum equations'). Explicit, closed-form analytical results have also been derived, giving V_r, V_θ and p as functions of two co-ordinates r and z. The theoretical model can predict torque, power output and efficiency, and compares well with experimental results. A hypothesis is proposed here that it may be possible to exploit the effects of intelligently designed and manufactured surface roughness elements to enhance the performance of a Tesla disc turbine.

Funding

References

1. Tesla N. Turbine. US Patent 1 061 206, 1913.
2. Hoya GP and Guha A. The design of a test rig and study of the performance and efficiency of a Tesla disc turbine. *Proc IMechE, Part A: J Power and Energy* 2009; 223(A4): 451–465.
3. Guha A and Smiley B. Experiment and analysis for an improved design of the inlet and nozzle in Tesla disc turbines. *Proc IMechE, Part A: J Power and Energy* 2010; 224: 261–277.
4. Guha A. A unified theory for the interpretation of total pressure and temperature in two-phase flows at subsonic and supersonic speeds. *Proc Roy Soc* 1998; 454: 671–695.
5. Guha A. Computation, analysis and theory of two-phase flows. *Aeronaut J* 1998; 102(1012): 71–82.
6. Steidel R and Weiss H. Performance test of a bladeless turbine for geothermal applications. Lawrence Livermore Laboratory, Report No. UCID-17068, 1974.
7. Rice W. Tesla turbomachinery. In: E Logan (ed.) *Handbook of turbomachinery*. New York: Marcel Dekker, 2003, pp.861–874.
8. Schroeder HB. *An investigation of viscosity force in air by means of a viscosity turbine*. BAE Thesis, Rensselaer Polytechnic Institute, 1950.
9. Rice W. An analytical and experimental investigation of multiple disk pumps and compressors. *ASME Trans J Eng Power* 1963; 85: 191–198.
10. Rice W. An analytical and experimental investigation of multiple-disk turbines. *ASME Trans J Eng Power* 1965; 87(1): 29–36.
11. Matsch L and Rice W. An asymptotic solution for laminar flow of an incompressible fluid between rotating disks. *ASME Trans J Appl Mech* 1968; 35(2): 155–159.
12. Boyack BE and Rice W. Integral method for flow between corotating disks. *ASME Trans L Basic Eng* 1972; 93: 350–354.
13. Breiter MC and Polhausen K. Laminar flow between two parallel rotating disks. ARL 62–318, Aeronautical Research Laboratory, OSR, USAF, Wright-Patterson AFB, 1962.
14. Boyd KE and Rice W. Laminar inward flow of an incompressible fluid between rotating disks, with full peripheral admission. *ASME Trans J Appl Mech* 1968; 35(2): 229–237.
15. Basset CE. An integral solution for compressible flow through disc turbines. In: 10th *Intersociety energy conversion and engineering conference*, Newark, DE, 18–22 August 1975.
16. Garrison PW, Harvey DW and Catton L. Laminar compressible flow between rotating disks. *ASME J Fluids Eng* 1976; 98: 382–389.
17. Cohen H, Rogers GFC and Saravanamuttoo HIH. *Gas turbine theory*, 4th ed. Harlow: Longman Group Ltd, Cornwall.
18. Walsh PP and Fletcher P. *Gas turbine performance*, 2nd ed. Oxford: Blackwell Science.
19. Guha A. Optimisation of aero gas turbine engines. *Aeronaut J* 2001; 105(1049): 345–358.
20. Guha A. Performance and optimization of gas turbines with real gas effects. *Proc IMechE, Part A: J Power and Energy* 2001; 215(4): 507–512.
21. Guha A. An efficient generic method for calculating the properties of combustion products. *Proc IMechE, Part A: J Power and Energy* 2001; 215(3): 375–387.
22. Guha A. Optimum fan pressure ratio for bypass engines with separate or mixed exhaust streams. *AIAA J Propul Power* 2001; 17(5): 1117–1122.
23. Guha A. Effects of internal combustion and nonperfect gas properties on the optimum performance of gas turbines. *Proc IMechE, Part C: J Mechanical Engineering Science* 2003; 217(9): 1085–1099.
24. Lemma E, Deam RT, Toncich D, et al. Characterisation of a small viscous flow turbine. *J Exp Therm Fluid Sci* 2008; 33: 96–105.
25. Deam RT, Lemma E, Mace B, et al. On scaling down turbines to millimetre size. *ASME Trans J Eng Gas Turbines Power* 2008; 130: 052301–052309.
26. Kandlikar SG, Schmitt D, Carrano AL, et al. Characterization of surface roughness effects on pressure drop in single-phase flow in minichannels. *Phys Fluids* 2005; 17: 100606–1–11.
27. Matveev YY and Pustovalov VN. Calculation of laminar flow of a viscous fluid between rotating disks. Transalated from *Izvestiya Akademii Nauk SSSR, Mekhanika Zhidkosti I Gaza.*, 1982, No. 1, pp.76–81.

28. Lawn MJ and Rice W. Calculated design data for the multiple-disk turbine using incompressible fluid. *ASME Trans J Fluids Eng* 1974; 96(3): 252–258.

29. Acheson DJ. *Elementary fluid dynamics*. Oxford: Clarendon Press, 1990.

Appendix 1

Notation

b	gap between two consecutive discs
k	isentropic index of fluid
$\dot{m}$	mass flow rate
p	pressure
P	modified pressure $= p - \rho g_z z$
p'	non-dimensional pressure $= \frac{p - p_2}{\rho \Omega^2 r_2^2}$
Q	volume flow rate
r	radial coordinate
R	non-dimensional radius (i.e. radius ratio) $= \frac{r}{r_2}$
U	absolute velocity of fluid
V	relative velocity of fluid
$\dot{W}_{th}$	theoretical ideal power output
$\dot{W}_{loss}$	overall loss in Tesla turbine
$\dot{W}_{act}$	theoretical power output with loss
z	axial coordinate
γ	tangential speed ratio $= \frac{\overline{U}_{\theta_2}}{\Omega r_2}$
Δp_{ic}	pressure drop between inlet and central exit of the rotor
ζ	non-dimensional average relative tangential velocity $= \frac{\overline{V}_\theta(r)}{\overline{V}_{\theta_2}}$
η	efficiency of the turbine
θ	Azimuthal direction in cylindrical co-ordinate system
μ	viscosity of the working fluid
ν	kinematic viscosity of working fluid (here the fluid is air)
ξ	non-dimensional average relative radial velocity $= \frac{\overline{V}_r(r)}{\overline{V}_{r_2}}$
ρ	density of the working fluid
τ_w	wall shear stress on one side of a single disc
ϕ_2	$\equiv \frac{\overline{V}_{r_2}}{\Omega r_2}$
Ω	rotational speed of the disc
$\Im$	torque on one side of a single disc
$\Im_{tot}$	total torque

Subscripts

r	component along the r-direction
z	component along the z-direction
θ	component along the θ-direction
1	central exit of the rotor
2	at rotor inlet

Overbar

$\overline{(\ )}$	z-averaged (z varies from 0 to b) flow variables

Appendix 2

1. Order of magnitude analysis of continuity equation

   For steady, laminar, incompressible flow and considering a relative frame of reference, the continuity equation in cylindrical co-ordinate system is

   $$\nabla \cdot \vec{V} = 0$$

   $$\frac{1}{r}\frac{\partial}{\partial r}(r V_r) + \frac{1}{r}\frac{\partial V_\theta}{\partial \theta} + \frac{\partial V_z}{\partial z} = 0$$

   According to assumption no. (4) enlisted in the 'Assumptions' section in the main text, $\frac{\partial V_z}{\partial z}$ term is neglected and considering assumption no. (3), $\frac{\partial V_\theta}{\partial \theta} = 0$. Therefore the simplified from of the continuity equation becomes

   $$\frac{1}{r}\frac{\partial}{\partial r}(r V_r) = 0$$

2. Order of magnitude analysis of θ momentum equation

   Neglecting the body force term along the θ direction (with assumption no. (6)), the θ momentum equation for incompressible flow[29] is

   $$\rho\left[\frac{DU_\theta}{Dt} + \frac{U_r U_\theta}{r}\right] = -\frac{1}{r}\frac{\partial p}{\partial \theta} + \mu\left[\nabla^2 U_\theta - \frac{U_\theta}{r^2} + \frac{2}{r^2}\frac{\partial U_r}{\partial \theta}\right]$$

   where

   $$\frac{DU_\theta}{Dt} = \frac{\partial U_\theta}{\partial t} + U_r\frac{\partial U_\theta}{\partial r} + \frac{U_\theta}{r}\frac{\partial U_\theta}{\partial \theta} + U_z\frac{\partial U_\theta}{\partial z}$$

   According to assumption no. (2), $\frac{\partial U_\theta}{\partial t} = 0$, considering assumption no. (3) $\frac{U_\theta}{r}\frac{\partial U_\theta}{\partial \theta} = 0$ and neglecting the term $U_z\frac{\partial U_\theta}{\partial z}$ with the help of assumption no. (4)

   $$\frac{DU_\theta}{Dt} = U_r\frac{\partial U_\theta}{\partial r}$$

Hence, the L.H.S. of the θ momentum equation becomes

$$\rho\left[U_r\frac{\partial U_\theta}{\partial r}+\frac{U_r U_\theta}{r}\right]$$

Now, in the R.H.S.

$$\nabla^2 U_\theta=\frac{\partial^2 U_\theta}{\partial r^2}+\frac{1}{r}\frac{\partial U_\theta}{\partial r}+\frac{\partial^2 U_\theta}{\partial z^2}+\frac{1}{r^2}\frac{\partial^2 U_\theta}{\partial \theta^2}$$

In the expression of $\nabla^2 U_\theta$, $\left(\frac{\partial^2 U_\theta}{\partial r^2}+\frac{1}{r}\frac{\partial U_\theta}{\partial r}\right)\ll\frac{\partial^2 U_\theta}{\partial z^2}$ (assumption no. (5)), and $\frac{1}{r^2}\frac{\partial^2 U_\theta}{\partial \theta^2}=0$ (assumption no. (3)).
Also in the R.H.S., $\mu\frac{2}{r^2}\frac{\partial U_r}{\partial \theta}=0$, $\frac{\partial p}{\partial \theta}=0$ (assumption no. (3)).
According to assumption no. (5), $\frac{U_\theta}{r^2}\ll\frac{\partial^2 U_\theta}{\partial z^2}$.
Taking all of the above considerations into account, the R.H.S. of the θ momentum equation can be approximated by $\mu\frac{\partial^2 U_\theta}{\partial z^2}$.
Substituting the relationship between the absolute and relative velocity the θ momentum equation becomes

$$V_r\frac{\partial V_\theta}{\partial r}+\frac{V_r V_\theta}{r}+2\Omega V_r=\nu\frac{\partial^2 V_\theta}{\partial z^2}$$

3. Order of magnitude analysis of z momentum equation

Considering assumption no. (4) z momentum equation becomes

$$\frac{\partial P}{\partial z}=0 \text{ (where, } P=p-\rho g_z z)$$

4. Order of magnitude analysis of r momentum equation

Neglecting the body force term along the r direction (with assumption no. (6)), the r momentum equation for incompressible flow[29] is

$$\rho\left[\frac{DU_r}{Dt}-\frac{U_\theta^2}{r}\right]=-\frac{\partial p}{\partial r}+\mu\left[\nabla^2 U_r-\frac{U_r}{r^2}-\frac{2}{r^2}\frac{\partial U_\theta}{\partial \theta}\right]$$

where

$$\frac{DU_r}{Dt}=\frac{\partial U_r}{\partial t}+U_r\frac{\partial U_r}{\partial r}+\frac{U_\theta}{r}\frac{\partial U_r}{\partial \theta}+U_z\frac{\partial U_r}{\partial z}$$

According to assumption (2) $\frac{\partial U_r}{\partial t}=0$, considering assumption (3) $\frac{U_\theta}{r}\frac{\partial U_r}{\partial \theta}=0$ and neglecting $U_z\frac{\partial U_r}{\partial z}$ with the help of assumption no. (4), $\frac{DU_r}{Dt}=U_r\frac{\partial U_r}{\partial r}$.
Hence the L.H.S. of the r momentum equation becomes $\rho\left[U_r\frac{\partial U_r}{\partial r}-\frac{U_\theta^2}{r}\right]$.

Now, in the R.H.S.

$$\nabla^2 U_r=\frac{\partial^2 U_r}{\partial r^2}+\frac{1}{r}\frac{\partial U_r}{\partial r}+\frac{\partial^2 U_r}{\partial z^2}+\frac{1}{r^2}\frac{\partial^2 U_r}{\partial \theta^2}$$

In the expression of $\nabla^2 U_r$, $\left(\frac{\partial^2 U_r}{\partial r^2}+\frac{1}{r}\frac{\partial U_r}{\partial r}\right)\ll\frac{\partial^2 U_r}{\partial z^2}$ (assumption no. (5)), and $\frac{1}{r^2}\frac{\partial^2 U_r}{\partial \theta^2}=0$ (assumption no. (3)).

Also in the R.H.S., $\mu\frac{2}{r^2}\frac{\partial U_\theta}{\partial \theta}=0$ (assumption no. (3)) and $\frac{\partial p}{\partial r}=\frac{\partial P}{\partial r}$ (assumption no. (6)), $\frac{\partial P}{\partial r}=\frac{dP}{dr}$ (as, $\frac{\partial P}{\partial \theta}=0$ and $\frac{\partial P}{\partial z}=0$), again, $\frac{dP}{dr}=\frac{dp}{dr}$ (assumption no. (6)).

According to assumption no. (5), $\frac{U_r}{r^2}\ll\frac{\partial^2 U_r}{\partial z^2}$.
Taking all of the above considerations into account, the R.H.S. of the r momentum equation can be approximated by $-\frac{dp}{dr}+\mu\frac{\partial^2 U_r}{\partial z^2}$.
Substituting the relationship between the absolute and relative velocity the r momentum equation becomes

$$V_r\frac{\partial V_r}{\partial r}-\Omega^2 r-2\Omega V_\theta-\frac{V_\theta^2}{r}=-\frac{1}{\rho}\frac{dp}{dr}+\nu\frac{\partial^2 V_r}{\partial z^2}$$

Appendix 3

1. Derivation of equation (17) from equation (2)

$$V_r\frac{\partial V_\theta}{\partial r}+\frac{V_r V_\theta}{r}+2\Omega V_r=\nu\frac{\partial^2 V_\theta}{\partial z^2}$$

The θ-momentum equation (2) is integrated partially with respect to z over the domain (0, $b/2$)

$$\int_0^{\frac{b}{2}}\left(V_r\frac{\partial V_\theta}{\partial r}\right)\delta z=\int_0^{\frac{b}{2}}\left(-\frac{V_r V_\theta}{r}\right)\delta z+\int_0^{\frac{b}{2}}(-2\Omega V_r)\delta z$$

$$+\int_0^{\frac{b}{2}}\left(\nu\frac{\partial^2 V_\theta}{\partial z^2}\right)\delta z$$

Substituting the definitions of R, ϕ_2 and γ as mentioned in the nomenclature, V_r from equation (10) and V_θ from equation (9), and integrating the resulting equation one obtains

$$\frac{d\zeta}{dR} = -\left\{\frac{1}{R} + 10 * \left(\frac{\nu}{\Omega b^2}\right) * \frac{R}{\phi_2}\right\}\zeta - \frac{10}{6(\gamma - 1)}$$

2. Derivation of equation (18) from equation (3)

$$V_r\frac{\partial V_r}{\partial r} - \Omega^2 r - 2\Omega V_\theta - \frac{V_\theta{}^2}{r} = -\frac{1}{\rho}\frac{dp}{dr} + \nu\frac{\partial^2 V_r}{\partial z^2}$$

$$\text{Or,} \ \frac{1}{\rho}\frac{dp}{dr} = -V_r\frac{\partial V_r}{\partial r} + \Omega^2 r + 2\Omega V_\theta + \frac{V_\theta{}^2}{r} + \nu\frac{\partial^2 V_r}{\partial z^2}$$

The *r*-momentum equation (3) is integrated partially with respect to z over the domain $(0, b/2)$

$$\frac{\Omega^2 r_2^2}{r_2}\int_0^{\frac{b}{2}}\frac{d\left(\frac{p-p_2}{\rho\Omega^2 r_2^2}\right)}{d\left(\frac{r}{r_2}\right)}\delta z \quad = \int_0^{\frac{b}{2}}-V_r\frac{\partial V_r}{\partial r}\delta z + \int_0^{\frac{b}{2}}\Omega^2 r\delta z$$

$$+ \int_0^{\frac{b}{2}}2\Omega V_\theta\delta z + \int_0^{\frac{b}{2}}\frac{V_\theta^2}{r}\delta z + \int_0^{\frac{b}{2}}\nu\frac{\partial^2 V_r}{\partial z^2}\delta z$$

Substituting the definitions of p', ϕ_2 and γ as mentioned in the nomenclature, V_r from equation (10) and V_θ from equation (9), and integrating the resulting equation one obtains

$$\frac{dp'}{dR} = R + 2(\gamma - 1)\zeta + \frac{6}{5}(\gamma - 1)^2\frac{\zeta^2}{R} + \frac{6}{5}\frac{\phi_2^2}{R^3} - 12\left(\frac{\nu}{\Omega b^2}\right)\frac{\phi_2}{R}$$